Optics and Lasers in Engineering 111 (2018) 222–226

Contents lists available at ScienceDirect

Optics and Lasers in Engineering

journal homepage: www.elsevier.com/locate/optlaseng

Intensity modulator fabricated in $LiNbO_3$ by femtosecond laser writing

D.A. Presti [a,b], V. Guarepi [a,c], F. Videla [a,c], A. Fasciszewski [d], G.A. Torchia [a,b,*]

[a] Centro de Investigaciones Ópticas, Camino Centenario y 506, M.B. Gonnet (1897), Bs. As., Argentina
[b] Depto. De Ciencia y Tecnología, Universidad Nacional de Quilmes, Roque Sáenz Peña 352, Bernal (1876), Bs. As., Argentina
[c] Facultad de Ingeniería, Universidad Nacional de La Plata, Calle 1 y 47, La Plata (1900), Argentina
[d] Departamento de Micro y Nanotecnología. Comisión de Energía Atómica (CAC), Av. Gral Paz y Constituyentes, San Martín (1650), Pcia. de Buenos Aires, Argentina

ARTICLE INFO

Keywords:
Mach Zehnder interferometer
Femtosecond laser writing
Lithium Niobate
Optical modulator circuits

ABSTRACT

This work presents the design, development and characterization of an integrated optical modulator based on a Mach Zehnder Interferometer (MZI) recorded inside x-cut Lithium Niobate (LNB) wafers. These optical circuits were fabricated by means of femtosecond laser writing on LNB samples under planar configuration. Electro-optics modulation was achieved by adding metal electrodes on the LNB sample surface, configured as a coplanar strip layout. The latter fabrication procedure was conducted by using standard lithography and sputtering techniques from silicon platform. The MZI prototypes developed support single mode propagation at communication wavelengths (1.55 μm) and present a half wave modulation voltage, $V\pi$, close to 45 V measured with a bias unbalance between arms of 15 V.

The MZI prototype has unique constructive features because it takes the advantages of the femtosecond laser writing. Additionally, it can be a key element of an opto-electronic device to be implemented in many systems, with high impact among others technological areas such as optical communication, sensing and control.

1. Introduction

The significant growth of fiber optic networks has strongly increased the manufacture and innovation of technological products in the communication area. In addition, this generates a constant increase of the requirements demanded by signal modulation systems to supply a dense flow of information. Nowadays the fiber optic networks exceed the 100 GHz of transmission rate. This technological advance constitutes a key element for the growth of optical communications [1–3].

The conventional signal modulators implemented in commercial fiber optics systems for transmitting internet signals, normally consist of an integrated Mach Zehnder interferometer. This commercial photonic device is manufactured based on optical waveguides, obtained by the well-known Titanium diffusion method on Lithium Niobate (LNB) wafers [4–7]. It is worth to mention that, because its electro-optical, acousto-optical and piezo-optical characteristic properties [8] LNB is a widely known material suitable for photonic devices.

In recent years a non-traditional technique to build optical circuits in optical materials has been developed. This technique has a great potential but not yet exploited as a standard manufacturing technology. This method is based on the interaction of ultra-short pulses of laser light with optical materials. One of the advantages of this technique is that it can be applied to a wide range of passive and active optical materials [9–17]. Additionally, it can be implemented in a single step allowing the construction of three-dimensional waveguides structures [9]. This favors better light guidance structures integration than the conventional methods which use flat structures, known as PLC (Planar Light wave Circuits) [2].

In this work we present an alternative development of an optical modulator based in a Mach Zehnder interferometer (MZI) integrated in Lithium Niobate (LNB) X cut wafers. The optical circuits were fabricated by means of femtosecond laser writing on LNB samples under planar configuration. The optical circuit was designed by considering the bend radius and the total length device in order to minimize the losses and reduce the $V\pi$ value. To validate the hypothesis, computational simulations were performed by using the RSOFT^{TM} commercial suite software. The electro-optics modulation was achieved by adding metal electrodes on the surface placed in the sample, through a technological platform commonly used for Silicon, based on lithography and sputtering techniques. Coupling of input and output of the MZ modulators into fiber optics were accomplished by performing an alternative integration procedure implemented with photo-cured adhesive and a homemade fiber hold system. Finally, the electro-optics modulator prototype was assembled in an own design holder that include a single mode fiber connectors type FC-APC at the input/output and four pins to voltage connection. The developed prototype supports single mode propagation at communications wavelengths (1.55 μm). The main operation characteristics ($V\pi$, modulation bandwidth, extinction ratio, insertion

* Corresponding author at: Centro de Investigaciones Ópticas, Camino Centenario y 506, M.B. Gonnet (1897), Bs. As., Argentina.
E-mail address: gustavot@ciop.unlp.edu.ar (G.A. Torchia).

https://doi.org/10.1016/j.optlaseng.2018.08.015
Received 7 May 2018; Received in revised form 17 August 2018; Accepted 18 August 2018

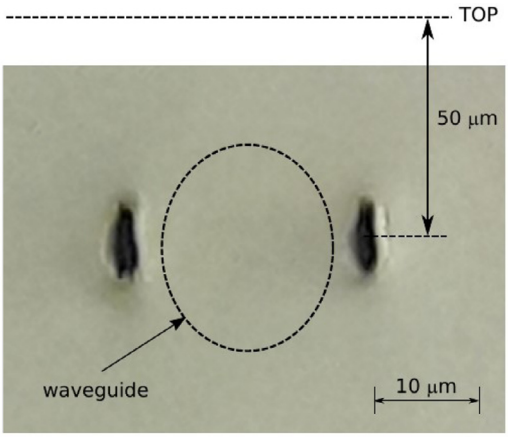

Fig. 1. Front view of the Type II waveguide end face. Black spots results from the laser focus along the writing process. Between them, enclosed by an oval shape, it is detailed the region where the refractive index is higher.

losses, etc.) will be reported in this paper.

2. Material and methods

2.1. Writing procedure

When a femtosecond laser pulse is focused in a transparent medium, structural and refractive index changes may be induced. These facts are caused by a non-linear absorption mechanism and affect only a narrow focal volume and its surroundings. This effect allows the direct writing structures in the material and constitutes the basic waveguide for the optical circuit studied. In particular, we have fabricated optical circuits using type II waveguides structures [10–12]. This process was done by a Chirp Pulsed Amplification (CPA) Titanium-Sapphire laser which emits 100 fs pulses at 800 nm wavelength and can deliver pulses up to 1 mJ of energy with 1 KHz of repetition rate. The laser beam parameters are configured according to the conditions of each experiment described below. The alignment is obtained by redirection and normal incidence on the sample. Finally, the incident laser beam is focused into the X cut $LiNbO_3$ sample by a 20X microscope objective (NA = 0.4) [13].

The structures made were recorded using a transverse writing geometry. This means that the laser pulses have a perpendicular incidence to the waveguide recorded direction (Y-axis). Knowing the optimal laser energy to obtain high performance waveguide structures in $LiNbO_3$ crystals [9], the laser energy is adjusted to a value of 0.7 μJ. The writing speed used was 30 μm/s. This value is set in order to obtain an optimal pulses superposition to make well defined waveguides and relatively homogeneous walls. A front view of the fabricated structures written with these parameters is shown in Fig. 1. This X cut Lithium Niobate waveguides support TM polarization modes.

2.2. Mach–Zehnder interferometer (MZI)

The MZI design consists of two branches with a balanced geometry. The laser writing strategy to draw our optical circuit was based on Type II structures. The waveguide was written in such a way that the propagation direction resulted parallel to the Y axis of the $LiNbO_3$ crystal. Double track separation gap of 23 μm ensured a single mode optical transmission at communication wavelengths. The total length of the optical circuit was 40 mm in a straight line. Fig. 2 shows in detail the dimensions of the optical circuit designed.

It is important to note that the design of a MZI should take into account losses caused by different origins, amongst we can mention: optical circuit bending, material losses (absorption), coupling factor, fluctuations of waveguide refraction index, waveguides roughness of each branch (scattering), etc.

In particular, the bend on each arm of the Mach Zehnder were designed using a sigmoidal shape and setting an aperture angle in agreement with the criteria established in reference [18]. Consequently, it can guarantee the least losses originated in bending.

2.3. Electrodes

The required electrodes for electro-optical modulation are deposited on the crystal surface by sputtering and by lithography techniques. In this process, first of all it was deposited a thin layer of titanium (50 nm) to hold it in the crystal and then a thicker layer of copper (350 nm). Geometry choice in the $LiNbO_3$ sample is essential to define the applied electric field direction, of course determined by the electrodes orientation.

It could be observed that the magnetic field belongs to a plane perpendicular to the crystal axis and the wave-vector k is almost grazing to the walls of waveguides (see Fig. 3a). When using this fabrication technique (laser direct writing) propagation takes place preferably for TM polarization modes [19]. In this case, the extraordinary refractive index (n_e) changes but not as much as the ordinary index (n_o). Moreover, these changes occur in different directions: n_o following the z axis, and n_e between the x and y axes [19,20].

Electrodes are necessary to apply an electric field on the horizontal axis (Z axis) to modify the refractive index according to the Pockels effect (Ec. 1) [18].

$$\Delta\left(\frac{1}{n^2}\right)_i = \sum_{j=1}^{3} r_{ij} E_j$$
$$\Delta n_e \approx \frac{n_{e^3} r_{33}}{2} E_z$$
$$\Delta n_o \approx \frac{n_{o^3} r_{13}}{2} E_z \quad (1)$$

If we consider optical modulation in the MZI up to 500 MHz, it is valid to use standard electrodes configuration instead of traveling wave electrodes commonly implemented for high speed rate [22]. The dimensions depicted in Fig. 3 shows the electrodes configuration in order to

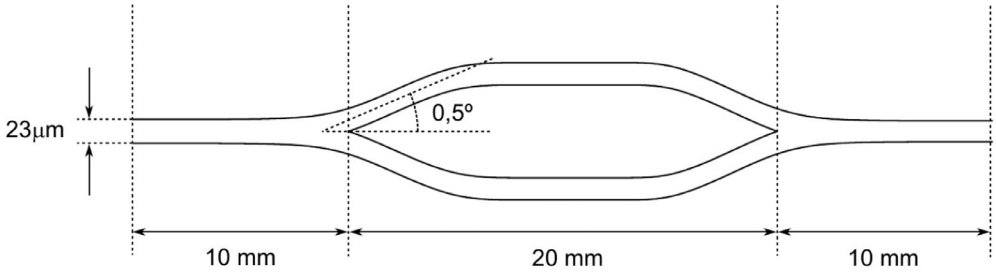

Fig. 2. Schematic geometry and dimensions of the whole MZI design. The length between arms bifurcations was of 20 mm. The represented angle was not made on a scale.

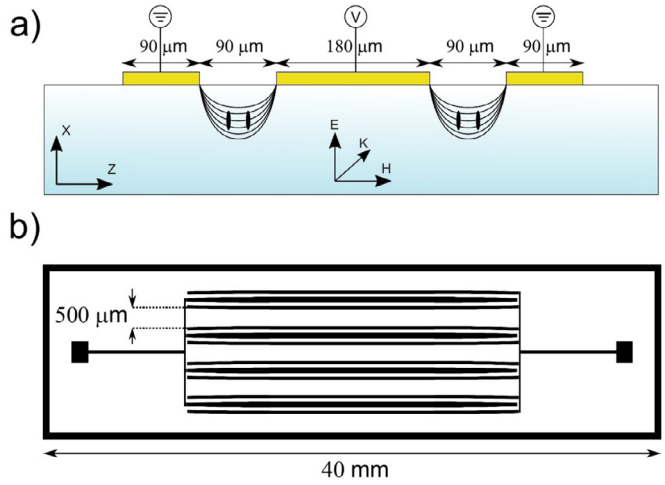

Fig. 3. Electrodes disposition: a) Schematic configuration, it can be appreciated the electrodes configuration and between them, the electric field in Z direction across the waveguides b) Top view of the mask for sputtering. We have implemented a set of four MZI only for test purposes. It can be noticed a slightly degree of curvature at the beginning and at the end of the electrodes in order to minimize the distance between them and the laser tracks.

produce symmetrical electric fields in both MZI arms. The central electrode width is bounded by the separation between MZI arms in turn related with the bending angle. For this type of structure we use an electrode configuration known as a *coplanar strip* and the voltage applied to this system corresponds to a *dual drive* electrode configuration type [23]. Each pair of electrodes has a separation of 90 µm and an active length of 20 mm on the waveguide surface. The electrodes separation was chosen taking into account electric field simulations considering the compromise between a reasonable low voltage and enough change in the refractive index. The active length of the electrodes is limited by the length of MZI arms. In the Fig. 3a) we can see a schematic front view of the system and in b) a top view of the electrodes configuration in the whole crystal. The design criterion was based on a redundancy strategy, so, several twin circuits were made in the same crystal.

2.4. Housing

Before making the experimental measurements, a robust holder was designed to have a final device for testing. This process includes the fiber optic and electrodes connection of input and output device and its housing. Only one MZI amongst the four implemented was optically connected. Alignment is critical for optical fiber connection to reduce losses. To build the device it is necessary an alignment process followed by fixing by means of photo curable optical adhesive. The electrical connection between electrodes and the output pins are made by using the wire bonding technique. Once the connections were made, the whole system was assembled in a holding case.

Fig. 4 shows a schematic of this final device. It shows the input /output optical fibers, the $LiNbO_3$ crystal, the electrodes and the electrical pins, respectively.

Finally, the whole set can be housed in a solid piece made of metal machined by a CNC router or in plastic using a 3D print technology. Holding case plays a double function: first it gives robustness and prevents against damage, and then, it immobilizes the internal components to maintain their alignment. This allowed us to manipulate the finished device under safe conditions for testing.

2.5. Measurement setup

Electro-optical modulation measurements were conducted by using the experimental set-up detailed in Fig. 5. As input device, we have used

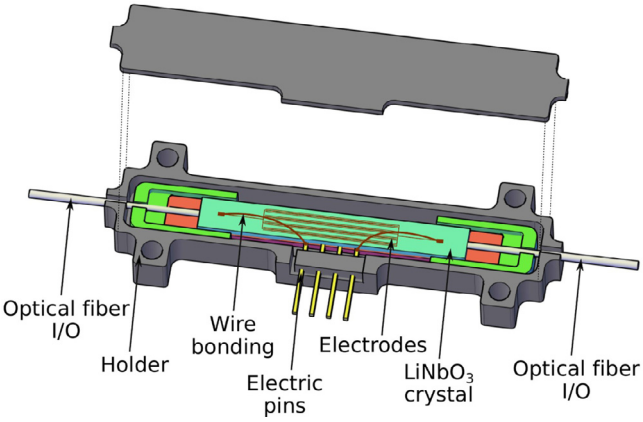

Fig. 4. Detailed of schematic final device. It can be observed two channels in the extremes of the case to align the optical fibers. Plate of $LiNbO_3$ crystal shows the deposited electrodes and the attached wire bonding for the voltage connections.

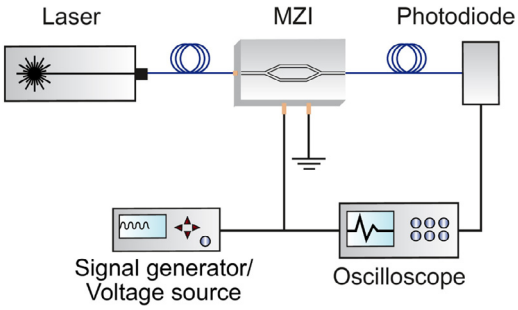

Fig. 5. Block diagram of the system used for the modulation test of the MZI. In black, electrical connections while in blue, optical connections by mean of fiber optics. (For interpretation of the references to colour in this figure legend, the reader is referred to the web version of this article.)

a Distributed FeedBack (DFB) laser diode operating in the communication band (1.55 µm, DFB QPhotonics - USA). It is connected to the device by using a single-mode fiber, while at the output, an InGaAs high-speed photo-diode (GPD Optoelectronics Corporation, USA) was used to measure the optical power. The electrical connection pins (for phase modulation test and consequently the amplitude) were connected to a signal generator (which injected ± 3 V peak-to-peak voltage sinusoidal signal to the MZI) and to a DC voltage source. The signals of the photodiode and the electrical input were both monitored in each experiment. This scheme allows us to obtain the main characteristic data of the device that we will analyze later.

3. Results and discussion

As a first analysis of the MZI systems, optical and electrical characteristics of electro-optics modulation were explored. In a first step, the MZI was analyzed in order to obtain the $V\pi$ voltage and the extinction ratio value. In this case, the procedure consisted in a sweep of DC voltage which was injected into the MZI electrical connection pins. Also, as a consequence, we obtained the imbalance between the interferometer branches. This value was determined considering the voltage necessary to obtain a maximum intensity at the MZI output. In addition we had obtained the half wave voltage value, resulting in a $V\pi \approx 45$ V. Although this value is considerably higher compared with the operation value observed in commercial MZ systems (less than 5 V), we would like to remark that it is expected to reach lower $V\pi$ values of this order if the MZI were manufactured on $LiNbO_3$ Z cut. This future implementation will guarantee a greater efficiency in the electro-optical effect, because in this last case the r_{33} coefficient will be responsible for the modula-

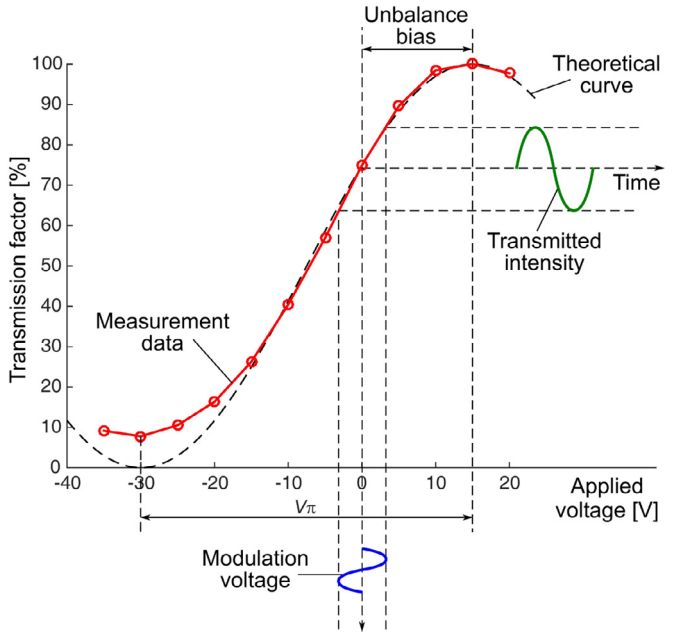

Fig. 6. Experimental values (red hole circles) of throughput of the electro-optic modulator as a function of the applied voltage. Additionally, the dashed line in grey shows the fitting curve corresponding to the MZI device analytical model. (For interpretation of the references to colour in this figure legend, the reader is referred to the web version of this article.)

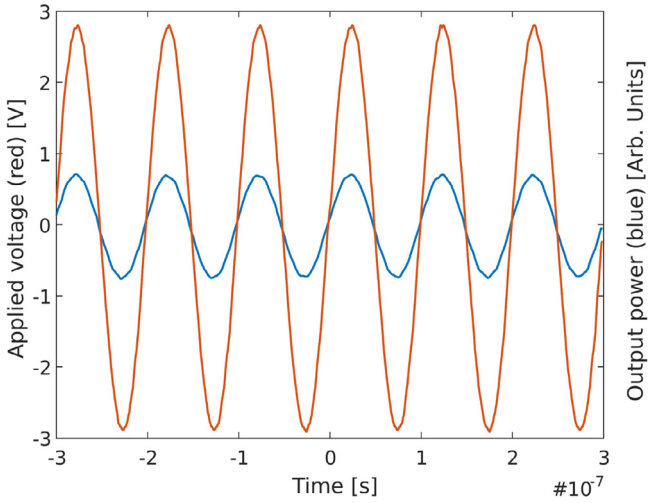

Fig. 7. Modulation tests of the MZI. The minimum of the optical signal (blue curve) correspond to the less value of power radiation (different from zero). The largest values of the modulus of applied voltage (red curve) are lower than Vπ, in spite of this, the degree of contrast is evident. (For interpretation of the references to colour in this figure legend, the reader is referred to the web version of this article.)

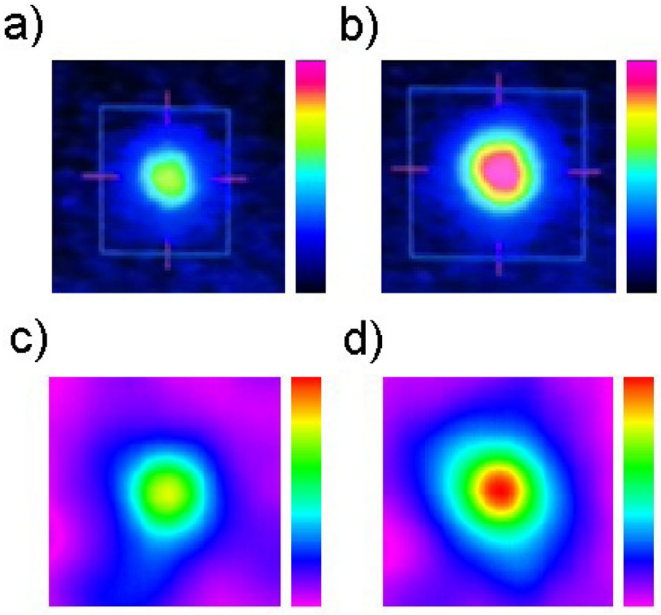

Fig. 8. a) Measured minimum optical modulation output mode, b) Measured maximum optical modulation output mode, c) and d) corresponding simulations of optical modes measured in a) and b). In both cases, modulation voltage was swept from -Vπ/2 to Vπ/2.

tion in the interferometer branches. This difference arises because the r_{31} coefficient has a value of 8.6, unlike r_{33} whose value is 30.8. The electro-optical effect is linked to this coefficient, therefore if the coefficient increases, the electro-optical effect will also increase [21].

In a second step of MZI analysis, taking into account the observed good performance by injecting a linear voltage signal as it is shown above; we proceeded to replace the direct current with a function generator source. This new configuration allows us to observe the system behavior with a modulated voltage input. This is the most common use of these devices. In order to analyze the response, in Fig. 6 we can see a retrieval of experimental data showing the characteristic sinusoidal form of the MZI throughput. These data were compared against the analytical expression of the transfer function [7]. The agreement between them is satisfactory, except in the first region corresponding to the minimum, where scattering defects originated in the writing process can distort the signal. Being the working zone the linear region, this distortion causes not effect, since is out of this region.

Considering the preliminary study for the MZI, we have injected a 10 MHz modulated voltage sinusoidal signal with amplitude of ~3 V. We remark that this kind of writing technique is not usually employed to make this type of device. In consequence we focused first in the feasibility of modulation instead of higher modulation rates. For higher modulation rates it is necessary to reconsider the electrodes configuration design.

In order to verify the behavior predicted, we can see in Fig. 7 the results obtained. In red and blue lines are represented both, the input voltage and the output optical signals respectively. The optical modulated output signal measured by the detector is recorded at the oscilloscope. As expected, the MZI signal at the output follow the shape of the electrical signal used to drive the electro-optical modulations. This fact is in agreement with the correct selection of a linear operative region. Additionally, phase shift between input and output signals is not observed, so reactive effects in metallic electrodes are negligible.

In order to complete the analysis, the photodiode was replaced from the experimental setup shown in Fig. 5, by a CCD camera. This allowed us to see the optical modes at the output of the MZI considering different transmission states driven by the modulated electrical signals at the input electrical pins. Figs. 8a) and b) shows the optical modes measured during the minimum and maximum modulation value. It is important to note that the color code scale for both figures is the same. Inspection of figures allows seeing the great difference in optical power between the two extremes analyzed. A similar analysis was reported in [20] but in our work the contrast was highly improved. Likewise the characteristics obtained by other techniques can be compared with our development as it is shown in Table 1. It can be noticed that, when Ti-diffusion process is employed, the guided modes are TE and the used electro-optic coefficient must be r33.

Table 1
Optical/Electrical characteristics of the MZI constructed in this work, compared with those developed by other authors and commercials.

Building technique	Material	Wavelength [μm]	Insertion losses [dB]	Vπ [V]	Ext. ratio [dB]	Un balance bias [V]	Full branching angle [°]	Ref.
Laser direct writing	$LiNbO_3$ X-cut	1.55	30	45	11	15	0.5	This work
Laser direct writing	$LiNbO_3$ X-cut	0.532	10	23	> 10	9.5	1.5	[20]
Ti-diffusion process	$LiNbO_3$ X-cut	1.525 – 1.605	4	7.5	20	–	–	[24]
Ti-diffusion process	$LiNbO_3$ X-cut	1.530 – 1.625	4	5	22	–	–	[25]

Figs. 8a) and b), corresponding to the measured modes, as we hope, are similar to the simulated ones shown in Fig. 8c) and d), however this fact is important because simulations do not include the effects of the fibre coupling to the $LiNbO_3$ crystal to perform the measure. Fibre could distort modes but this was not observed. In summary mode distribution seems to be few dependent from the fibre in both branches, being suitable to achieve a good degree of contrast when interference take place. The variation of refractive index due to the applied voltage was estimated in $\Delta n \sim 1.5 \times 10^{-5}$, this result was obtained from simulations.

4. Conclusions

Femtosecond laser writing has demonstrated potential for optical circuit fabrication and relative advantages respect to the conventional technologies. Amongst them we can mention, fast prototyping, feasibility, repeatability and 3D architecture capability.

In particular, we have presented a prototype model of an integrated amplitude modulator based on a Mach Zehnder Interferometer (MZI). This design and development were made in X cut Lithium Niobate crystals wafers and has reached an appropriate optical performance. The fabricated device has shown a correct functionality and design showing that electro-optical effect is a suitable for achieving optical signal modulation for the frequency rate used.

The design of the metallic electrodes deposited on both sides of the MZI branches show a good performance to control the refractive index values. The determined value of Vπ was approximately 45 V and an interferometer imbalance (bias) of 15 V. Although 45 V is a comparatively high value for Vπ considering versions of MZI made with other techniques, we have proposed an alternative using a Z cut LNB crystal allowing to diminish this voltage around 4 times. No phase shifting could be observed between optical signal and the control signal applied to the electrodes. This modulation technique allows extinction ratios of 11 dB and the optical mode observed remain invariable considering the amplitude spanning region. It was shown that few influences over the mode distribution can be assigned to fibre coupling.

The developed device was packaged with robustness enhancing its opto-mechanical connectivity, consequently achieving reproducibility in the measuring of its parameters. Additionally, it highlights the manufacturing technique and enables the possibility of improving preliminary designs to adapt the devices to the different requirements of new optical systems.

Acknowledgment

This work was partially supported by the Agencia Nacional de Promoción Científica y Tecnológica (Argentina) under the project PICT-2016-4086. FV belongs to the Comisión de Investigaciones Científicas (Buenos Aires, Argentina). GAT and DP are with CONICET, Argentina.

References

[1] Kaminow IP, Li T, Willner AE. Optical fiber telecommunications V B.. California, USA: Elsevier; 2008.
[2] Lam CF. Passive optical networks. California, USA: Elsevier; 2007.
[3] Shami A, Maier M. Broadband access network: Technologies and Deployments.. New York, USA: Springer; 2009.
[4] Lifante G. Integrated photonics: fundamentals. West Sussex, England: Wiley; 2003.
[5] Korkishko YN, Fedorov VA, Kostritskii SM, Alkaev AN, Paderin EM, Maslennikov EI, Apraksin DV. Multifunctional integrated optical chip for fiber optical gyroscope fabricated by high-temperature proton exchange. In: Proc. SPIE 4944, Integrated Optical Devices: Fabrication and Testing; 2003.
[6] Becker P, Brinkmann R, Dinand M, Sohler W, Suche H. Er-diffused Ti:LiNbO3 waveguide laser of 1563 and 1576nm emission wavelengths. Appl Phys Lett 1992;61:1257.
[7] Noguchi K. Lithium Niobate Modulators. Broadband optical modulators: science, technology and applications. Chen A, Murphy E, editors. Florida, USA: CRC Press; 2012.
[8] Tomeno I, Matsumura S, Florea C. Stiffness and compliance of LiNbO3. In: Wong KK, editor. Properties of lithium niobate. United Kingdom: INSPEC the Institution of Electrical Engineers; 2002. p. 57–60.
[9] Osellame R, Cerullo G, Ramponi R, editors. Femtosecond laser micromachining. Berlin: Springer-Verlag; 2012.
[10] Chen F, Vazquez JR. Optical waveguides in crystalline dielectric materials produced by Femtosecond-Laser micromachining. Laser Photonics Rev 2014;8:251–75.
[11] Li Lingqi, Nie Weijie, Li Ziqi, Lu Qingming, Romero Carolina, Vázquez de Aldana JavierR, Chen Feng. All-laser-micromachining of ridge waveguides in LiNbO3 crystal for mid-infrared band applications. Sci Rep 2017;7:7034.
[12] Lv Jinman, Cheng Yazhou, Lu Qingming, Vázquez de Aldana JavierR, Hao Xiao–Tao, Chen Feng. Femtosecond laser written optical waveguides in z-cut MgO:LiNbO3 crystal: fabrication and optical damage investigation. Opt Mater 2016;57:169–73.
[13] Peyton R, Guarepi V, Videla F, Torchia GA. Key kinematic parameters in a low-loss power splitter written by Femtosecond Laser micromachining. J Micromech Microeng 2018;28(5).
[14] Torchia GA, Ródenas A, Benayas A, Roso L, Jaque D. Highly efficient laser action in femtosecond-written Nd:yttrium aluminum crystals. Appl Phys Lett 2008;92:111103.
[15] Méndez C, Vázquez de Aldana JR, Torchia GA, Roso L. Arrays of guiding structures induced in fused silica by void like defects using femtosecond laser pulses. Appl Phys B Laser Opt 2007;86:243.
[16] Dong Ning-Ning, Martinez de Mendivil J, Cantelar E, Lifante G, Vazquez de Aldana JR, Torchia GA, Chen F, Jaque D. Self-frequency-doubling of ultrafast laser inscribed Neodymium Doped Yttrium Aluminum Borate waveguides. Appl Phys Lett 2011;98:181103–5.
[17] Biasetti D, Neyra E, Vázquez de Aldana JR, Roso L, Torchia GA. Buried waveguides in Nd:YLF crystals obtained by femtosecond laser writing under double line approach. Appl Phys A 2013;110:595.
[18] Guarepi V, Perrone C, Aveni M, Videla F, Torchia GA. Bending waveguides made in x-cut lithium niobate crystals for technological applications. J Micromech Microeng 2015;25:125023.
[19] Tejerina MR, Biasetti DA, Torchia GA. Polarization behaviour of femtosecond laser written waveguides in lithium niobate. Opt Mater 2015;47:34–8.
[20] Ringleb S, Rademaker K, Nolte S, Tünnermann A. Monolithically integrated optical frequency converter and amplitude modulator in linbo3 fabricated by femtosecond laser pulses. Appl Phys B 2010;102(1):59–63.
[21] Yariv A, Yeh P. Photonics: optical electronics in modern communications. New York, USA: Oxford University Press; 2007.
[22] Gopalakrishnan GK, Burns WK, McElhanon RW, Bulmer CH, Greenblatt AS. Performance and modeling of broadband LiNbO3 traveling wave optical intensity modulators. J Lightwave Technol 1994;12:1807–18.
[23] Knorr JB, Kuchler K. Analysis of coupled slots and coplanar strips on dielectric substrate. IEEE Trans Microwave Theory Tech 1975;23:541–8.
[24] Thorlabs products. Lithium Niobate Modulators, LN81S-FC - Zero-Chirp, 10 GHz Intensity Mod., Integrated PD and Replaceable GPO Conn, FC/PC. [accessed 21 June 2018] https://www.thorlabs.com/thorproduct.cfm?partnumber=LN81S-FC.
[25] Ixblue products. Lithium Niobate electro optic modulator: intensity modulators: MX-LN-10. [accessed 21 June 2018] https://photonics.ixblue.com/product-detail/mx-ln-10.